The Global Distribution of Supersaturation in the Upper Troposphere from the Atmospheric Infrared Sounder

ANDREW GETTELMAN

National Center for Atmospheric Research, Boulder, Colorado*

ERIC J. FETZER, ANNMARIE ELDERING, AND FREDRICK W. IRION

NASA Jet Propulsion Laboratory, California Institute of Technology, Pasadena, California

(Manuscript received 3 August 2005, in final form 31 March 2006)

ABSTRACT

Satellite data from the Atmospheric Infrared Sounder (AIRS) is analyzed to examine regions of the upper troposphere that are supersaturated: where the relative humidity (RH) is greater than 100%. AIRS data compare well to other in situ and satellite observations of RH and provide daily global coverage up to 200 hPa, though satellite observations of supersaturation are highly uncertain. The climatology of supersaturation is analyzed statistically to understand where supersaturation occurs and how frequently. Supersaturation occurs in humid regions of the upper tropical tropopause near convection 10%–20% of the time at 200 hPa. Supersaturation is very frequent in the extratropical upper troposphere, occurring 20%–40% of the time, and over 50% of the time in storm track regions below the tropopause. The annual cycle of supersaturation is consistent for the ~2.5 yr of data analyzed. More supersaturation is seen in the Southern Hemisphere midlatitudes, which may be attributed to higher temperature variance.

1. Introduction

The presence of regions in the atmosphere that are supersaturated with respect to ice has been known since the 1940s (Glückauf 1945; Brewer 1946). Molecules of water do not simply lock together in an ice lattice of their own accord at saturation pressures, but either require a surface to condense on to or require conglomerations of water molecules as liquid to freeze. Thus it is not surprising to expect relative humidities over ice (RHi) in excess of 100% (i.e., supersaturation). Theoretically, supersaturation may be observed up to the saturation vapor pressure over water. Supersaturation in the upper troposphere can be inferred from the presence of persistent contrails behind aircraft, which require humidities above that of ice saturation to form (Appleman 1953; Schumann 1996).

Supersaturation is critical for understanding the process of ice cloud formation. This process, which is also affected by the presence or absence of atmospheric particles (aerosol), has implications for the radiative balance of the climate system through its affect on clouds (longwave cloud forcing) and water vapor (water vapor feedbacks). Most global models of the climate system do not permit supersaturation but instead dictate full condensation of all water vapor to maintain a vapor pressure less than 100% over ice at temperatures where only ice exists (typically below −20° to −40°C). Understanding the distribution of water vapor close to and beyond ice saturation is thus important for simulating and predicting future climate and the impacts of anthropogenic influences on ice clouds. These impacts include changes in aerosol that affect ice nuclei, or aircraft emissions of particles and water vapor directly into the upper troposphere.

In recent years supersaturated conditions (RHi > 100%) both inside and outside of clouds have been observed extensively from aircraft, balloons, and satellites. During the Stratosphere Troposphere Exchange Project (STEP), supersaturation was observed near the tropical tropopause from in situ research aircraft by

* The National Center for Atmospheric Research is sponsored by the National Science Foundation.

Corresponding author address: Andrew Gettelman, National Center for Atmospheric Research, 1850 Table Mesa Drive, Boulder, CO 80305.
E-mail: andrew@ucar.edu

Kelly et al. (1993). Supersaturation in midlatitudes from research aircraft was reported by Heymsfield et al. (1998) during the Subsonic Aircraft: Contrail and Cloud Effects Special Study (SUCCESS) aircraft campaign. Gierens et al. (2000) analyzed data taken from commercial aircraft and found extensive supersaturation in the upper troposphere. Ovarlez et al. (2002) reported supersaturation inside and outside of cirrus clouds for the Northern and Southern Hemisphere from in situ aircraft during the Interhemispheric Differences in Cirrus Properties from Anthropogenic Emissions (INCA) campaign. Jensen et al. (2000) describe supersaturated conditions from several NASA aircraft campaigns in the Tropics and midlatitudes, and Jensen et al. (2005) describe humidities approaching water saturation (~200% RHi) from the recent aircraft measurements.

In addition to aircraft measurements, balloons and satellites can also observe supersaturation. Supersaturation has been observed from balloonborne hygrometers in the Tropics by Vömel et al. (2002). Spichtinger et al. (2003a) found supersaturation in radiosonde measurements over midlatitudes (Germany).

From in situ data, it has been estimated that ice supersaturated regions, at least in Northern Hemisphere midlatitudes, are typically 150 km in horizontal extent with a distribution strongly skewed toward smaller sizes (Gierens and Spichtinger 2000) and 0.5 km ± 0.6 km in vertical extent (Spichtinger et al. 2003a). Given this scale, it is not unreasonable to see some of these regions from satellites, even given their broad weighting functions, despite inherent difficulties with retrieving supersaturation from remote sensing instruments (Buehler and Courcoux 2003). Jensen et al. (1999) and Spichtinger et al. (2003b) reported supersaturation in RHi data from the Microwave Limb Sounder (MLS) on the Upper Atmosphere Research Satellite (UARS), though cloud contamination may affect these retrievals (Read et al. 2001). Gierens et al. (2004) also found evidence of supersaturation in a reanalysis of Television Infrared Observation Satellite (TIROS) Operational Vertical Sounder (TOVS) data over Europe despite the 3–5-km vertical weighting function.

In this work we use newly available satellite observations from the Atmospheric Infrared Sounder (AIRS) to develop a global climatology of supersaturation in the upper troposphere up to 200 hPa. Unfortunately, this does not include the Tropical tropopause layer (TTL). AIRS data and uncertainties are described in section 2, comparisons with other observations are presented in section 3, and the climatology of supersaturation is illustrated in section 4. Discussion of key points is in section 5 and conclusions are in section 6.

2. Data description

Relative humidity data is derived from the AIRS instrument on the NASA *Aqua* satellite, as discussed by Gettelman et al. (2006). We restate the key points here. AIRS is a nadir infrared and microwave sounder with ~2000 independent channels and nine separate pixels, which enable retrieval of a profile of temperature and water vapor in the presence of up to 70% effective cloud fraction (Aumann et al. 2003), where cloud fraction is the product of area and emissivity. No data is available if the retrieval detects sufficiently opaque cloud (the surface temperature deviates from what is expected based on correlative data). We use AIRS level-2 data retrievals (version 3.0; Fetzer et al. 2003) with an effective vertical resolution of 1–3 km (Susskind et al. 2003). Horizontal resolution is approximately 45 × 45 km (nine pixels of 15 × 15 km each), and there are on the order of 300 000 AIRS profiles per day. AIRS is in a polar orbit with fixed equatorial local (solar) crossing times of ~1330 and ~0130.

Retrieved profiles of water vapor (specific humidity) and temperature are used to derive relative humidity for each profile. Retrievals provide the column water vapor between two pressure levels ($\overline{q}$) and temperature on pressure levels. We construct relative humidity by dividing the column water vapor by a saturated vapor column ($\mathrm{RH} = \overline{q}/\overline{q}_s$). The saturated vapor column ($\overline{q}_s$) is estimated by numerically integrating the saturation vapor pressure, assuming that temperature in the layer is linear between the two layer edges. We have conducted a detailed sensitivity test of the method of calculating relative humidity, and the results are not highly sensitive to the method chosen.

The saturation vapor pressure is calculated using the formulation of Goff and Gratch (1946) over water for temperatures >273 K (0°C) and over ice for temperatures <253 K (−20°C), with a linear combination of the two between them. We choose this "merged" relative humidity (and refer to it as simply relative humidity or RH) because it is typical of the formulation used for general circulation models of the atmosphere used in reanalyses and climate studies. Practically, for most of the upper-tropospheric data shown here, temperatures are well below −20°C (253°K), and RH is equivalent to relative humidity over ice (RHi). Uncertainties in the saturation vapor pressure at temperatures 220 K and above are less than 1% (Murphy and Koop 2005). Following the AIRS convention, pressures here refer to the bottom of the layer.

AIRS data validation is ongoing, but data have been found to be of high quality. Tobin et al. (2006) compared AIRS retrievals with dedicated radiosondes over

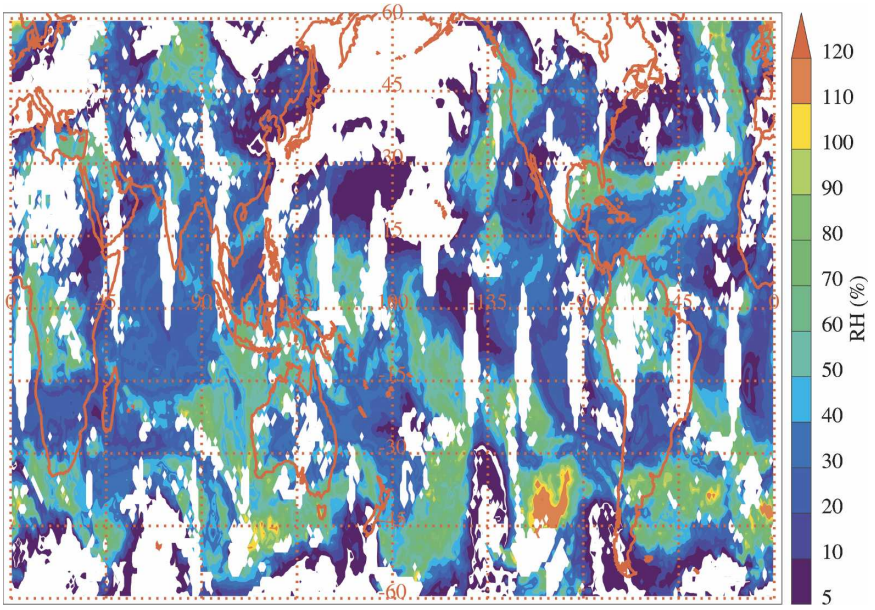

FIG. 1. AIRS relative humidity (%) for 6 March 2005 from 60°S to 60°N latitude at 250 hPa. Missing data in white.

midlatitudes and tropical oceans and found rms differences of ~1 K (less over ocean) for temperature and ~20% for specific humidity. Divakarla et al. (2006) found similar results in comparison with the global operational radiosonde archive. Radiosonde sensors in the upper troposphere however are themselves prone to some biases (Miloshevich et al. 2006).

Previous comparison of AIRS data with in situ research aircraft in the tropical upper troposphere up to 200 hPa by Gettelman et al. (2004) indicate that the standard deviation (σ) of AIRS data from in situ data is less than 1.5 K for temperature, ~20% for water vapor, and ~20% for relative humidity, but only 9% for RH at 250 hPa and below. The scatter is based on detailed comparisons of collocated satellite data with aircraft humidity averaged over the same distance for 40 individual flight legs from 200 to 500 hPa (see Gettelman et al. 2004 for more details). None of the observations show an obvious bias. Relative humidity uncertainty (9%) is less than would be expected from simply adding temperature and water vapor errors (~30%), which indicates some cancellation in uncertainty, or that the scatter is not normally distributed, though the statistics (only ~40 corresponding 100-km flight segments) are barely significant.

A resulting map for one day of gridded relative humidity data is illustrated in Fig. 1. Data values are missing for 1) near-equatorial points where orbit tracks do not overlap, 2) locations of thick clouds (where no retrieval is performed), and 3) large sections of the extratropical lower stratosphere where water vapor is below the retrieval threshold and does not meet quality control checks. A detailed analysis of locations of supersaturation indicates that high values of RH are found associated with deep convection in the Tropics (the western Pacific, Africa, and South America show up prominently) and with midlatitude storm systems (extratropical cyclones). Supersaturation is often seen at the leading edge of baroclinic storms, associated with fronts in midlatitudes, or occasionally embedded within frontal cloud bands, though more often at the edge of these bands or occasionally behind them. Supersaturation from AIRS is only rarely seen in clear sky regions without upper-level clouds. Supersaturation also does not appear as pixelated "noise" in individual profiles, but over coherent regions.

Data from September 2002 through March 2005 (31 months) are used to produce probability distribution functions (PDFs) of relative humidity in Fig. 2. Data from 60°S to 60°N latitude and from 600 to 200 hPa are shown in Fig. 2, annually and seasonally averaged. This represents on the order of 200 million profiles. The right panel is the same data, but displayed with a logarithmic vertical axis. Overall, the PDF is peaked toward low RH, reflecting the large area of subtropical and tropical dry regions. A total of 4% of the data indicate RH (merged over ice and water) greater than 100%. Supersaturation up to 250% over ice (thought to be physically implausible) is indicated in the raw data on rare occasions. The right panel indicates that, over most

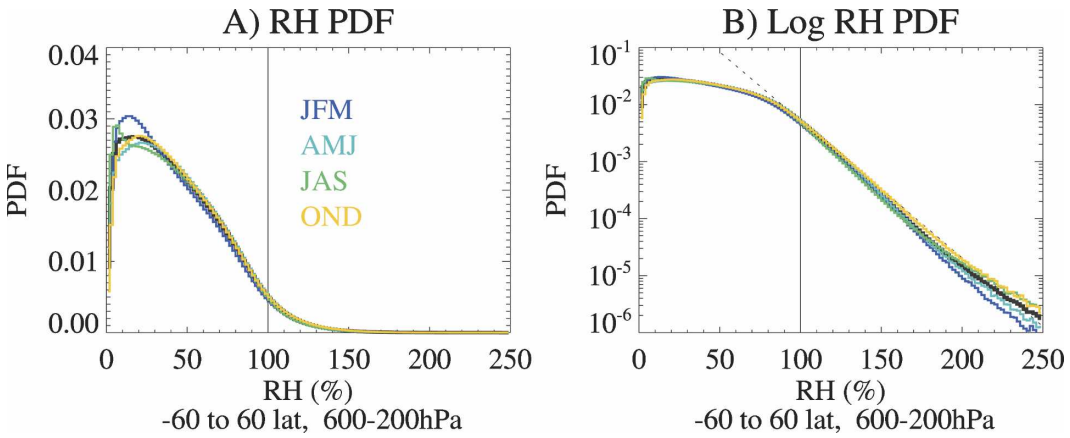

FIG. 2. Probability distribution function of RH from 60°S to 60°N and 600 to 200 hPa from AIRS data for 2003 and 2004. Black line is the annual average; colored lines are seasonal averages for January–March (purple), April–June (blue), July–September (green), and October–December (yellow): (left) Linear scale and (right) a log scale of the same data. Dotted line in the right panel is an exponential fit with exponent of −0.06.

of the range of supersaturation, the data is well described by an exponential fit with an exponent of −0.06 (the dotted line in Fig. 2b).

Obviously, errors in the temperature and water vapor retrievals will create uncertainties in the estimation of relative humidity. It is entirely possible that errors in the data might create additional supersaturation where none exists. To investigate this uncertainty, we take RH data from a simulation of the National Center for Atmospheric Research (NCAR) Community Atmosphere Model version 3 (CAM3) and perturb it in two ways: 1) with a random error sampled from a normal distribution with standard deviation of 9% [the statistical 1σ uncertainty in RH below 200 hPa found by Gettelman et al. (2004)] and 2) individual uncorrected errors in temperature and specific humidity sampled from normal distributions with standard deviations 1.5 K and 20% (the uncertainty from the aircraft comparisons). The model is described by Collins et al. (2006). The important point for this analysis is that the model explicitly does not allow supersaturation. This Monte Carlo approach is similar to that taken by Buehler and Courcoux (2003).

The AIRS PDF for 40°–60°N latitude is shown in black in Fig. 3. The PDF of model-simulated RH in midlatitudes is shown in dark gray in Fig. 3. The PDF is limited to a maximum RH of 100%. Model RH is calculated over ice and liquid the same way as for the AIRS data. The perturbed data is shown in light gray for (i) 9% RH uncertainty (solid light gray) and for (ii) individual temperature and water vapor uncertainty (dashed light gray). Overall, supersaturation in the region is found in 5% of the AIRS data, 0% of the unperturbed model data, 4% of the perturbed model data for (i), and 10% of the perturbed data for (ii). Thus, if the satellite data has normally distributed uncorrelated errors, it is possible that a majority of supersaturation observed could be spurious.

The high potential uncertainty of satellite data indicated in Fig. 3 makes interpretation of the satellite data difficult. Supersaturation measured from AIRS is occurring in a volume of ~45 km by ~45 km horizontally and ~2 km vertically. If typical sizes of supersaturated regions in the upper troposphere observed by aircraft are ~150 km in the horizontal (Gierens and Spichtinger 2000; though as noted many regions may be smaller than this) and from radiosondes are 0.5–1 km in the vertical (Spichtinger et al. 2003b), it is not unreasonable

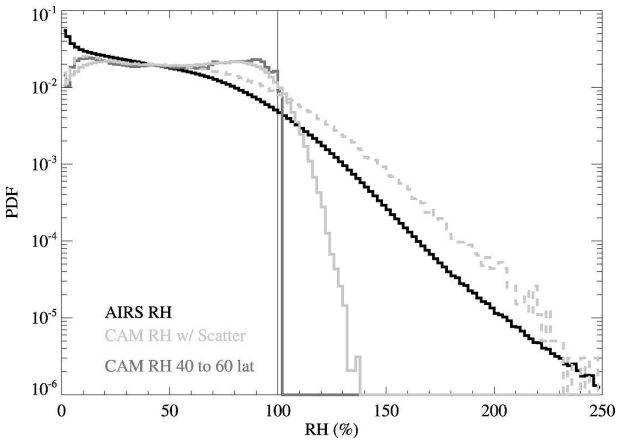

FIG. 3. Midlatitude PDFs of RH from 40° to 60°N and 600 to 200 hPa for all months of the year. AIRS data in black, CAM3 output in dark gray, and CAM3 with scatter in light gray: Solid line represents 9% RH standard deviation; dashed line represents temperature and specific humidity errors as described in the text.

to expect to see at least some supersaturated regions. The largest uncertainty is likely to be due to the vertical weighting function of AIRS, which is thicker than many of the layers may be. Thus, we note a significant caveat on this study: AIRS "supersaturation" is a large-scale quantity. It is not the same supersaturation that would be felt by cloud particles since there is likely significant finescale structure in the humidity fields in three dimensions, whereas the satellite will only measure a horizontal and vertical "average" temperature or total column specific humidity assuming uniform distribution. However, the large-scale relative humidity is a useful quantity to use as an attempt to understand the global distribution of supersaturated regions. The problem is characteristic of all attempts at measuring supersaturation (the tail of the RH distribution) with remote sensing.

It is difficult to quantify the level of supersaturation from this data and relate it to cloud microphysics. So, in this work we turn to a statistical quantity: the frequency (or fraction) of observed supersaturation. This quantity is directly relevant for understanding persistent contrails and cirrus clouds, though perhaps not directly relevant for understanding ice nucleation processes. Based on the high potential uncertainty noted in Fig. 3, the frequency of supersaturation is uncertain by up to 100%. Statistically we cannot demonstrate that any supersaturation exists at all in AIRS data, a similar conclusion to that reached by Buehler and Courcoux (2003) with MLS data. As a result, we proceed with caution, and in the next section we will perform more comparisons between AIRS observations of supersaturation and other measurements to show that the supersaturation frequency observed from AIRS appears to be geophysical.

3. Comparisons with aircraft and balloon observations

In this section we compare AIRS RH observations to other available observations of relative humidity from in situ aircraft in the upper troposphere and balloons. We use three different sets of data. First we compare with research aircraft data, which have high precision, but limited sampling and then compare with data from balloon hygrometers. We also examine data from in-service commercial aircraft, which have less precision, but greater sampling.

First we compare AIRS observations of supersaturation with in situ data from a research aircraft. We use the same data as Gettelman et al. (2004) from the Preliminary Aura Validation Experiment (PreAVE), conducted using the NASA WB57 aircraft. The campaign was based in Houston, Texas, and San Jose, Costa Rica. The flight latitudes ranged from approximately 5°S to 30°N and flight dates from 16 January to 2 February 2004. Details of the data and instruments are described by Gettelman et al. (2004). In contrast to the scatterplots along flight tracks shown by Gettelman et al., which require averaging over 100 km or so, we show high-resolution data in Fig. 4 for points within the vertical sampling range of AIRS (up to 200 hPa), which is below the aircraft cruise altitude, so this data represents only several ascents, decents, and dives. Data is from three different instruments. Harvard water vapor and total water are described by Weinstock et al. (1994). The Jet Propulsion Laboratory laser hygrometer (JLH) measuring water vapor is described by May (1998). Quoted uncertainty for the Harvard water vapor instrument, as validated by laboratory calibrations, in-flight intercomparisons with JLH (May 1998), and in situ vacuum ultraviolet absorption, is ±5%. The data have occasional significant differences, with the Harvard instruments (10-s data) showing saturation for 8% of the points and the JLH instrument (1-s data) having a similar distribution and range, but with supersaturation only 1% of the time. Statistics for clear-sky points only (estimated in Fig. 4 in red where the ratio of total water to water vapor is less than 1.1) are similar because most of this mission was conducted in regions without clouds. Overplotted is the AIRS climatology for this region of the tropical and subtropical eastern Pacific for January–March (the curve is not very sensitive to the particular region boundaries or to the time average). AIRS data are supersaturated 1% of the time. RHi > 160% is not physical at these altitudes and data beyond this range are likely due to noise (though, since this is a log scale, the number of points in this region is small). AIRS and aircraft PDFs have similar slopes throughout the entire range of the data. Statistically, AIRS is producing reasonable results relative to these data for supersaturated points, though this campaign does not provide enough statistics to reliably estimate a PDF, nor because of spatial sampling differences do we necessarily expect the PDFs to be the same.

Supersaturation is seen frequently from balloons. Frost-point hygrometer data from Vömel et al. (2002) indicates that in the layer 2 km below the tropopause supersaturation is seen on all 14 flights in the tropical western Pacific and on just over 50% (7 of 12 flights) in the tropical eastern Pacific. These data are not directly comparable to AIRS data since AIRS does not observe this region (it is above 200 hPa). High-latitude balloon flights from the same instrument at 60°–70°N (H.

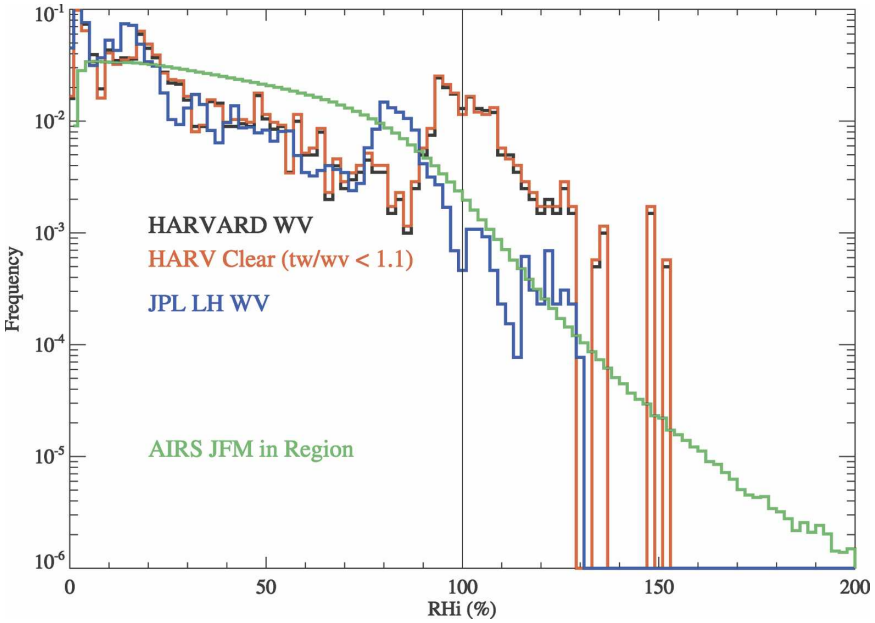

FIG. 4. PDFs of RH from the PreAVE experiment in January–February 2004 for altitudes 600–200 hPa. Harvard water vapor (black), Harvard water vapor sorted by Harvard total water for clear sky (red), and JPL laser hygrometer (blue). AIRS RH PDF from January–March and 5°S–20°N, 110°W–80°W (green).

Vömel 2005, personal communication) indicate that supersaturation is seen in the layer 2 km below the extratropical tropopause 67% of the time (30 of 45 flights). In the same region, AIRS sees supersaturation in the upper troposphere 40%–70% of the time. This is not a robust statistical comparison due to the small sample of balloons. The frost point hygrometer described here was noted to be up to 20% drier than the aircraft instruments described above in the upper troposphere/lower stratosphere (UT/LS) region (K. H. Rosenlof 2005, personal communication).

The Measurement of Ozone and Water Vapor by Airbus In-Service Aircraft (MOZAIC) project has been taking observations of humidity for the last 10 years. The project is described by Marenco et al. (1998), and the humidity observations are described by Helten et al. (1998). To measure humidity, MOZAIC uses a modified humidicap sensor in a housing on the aircraft. The air undergoes significant compressional heating upon measurement, which is empirically corrected. It is thus not a reference instrument for humidity measurement in the upper troposphere. However, MOZAIC has nearly 1500 flights a year, concentrated in the Northern Hemisphere along flight routes from Europe.

We have performed detailed comparisons averaging MOZAIC data in 100-km flight segments and comparing to AIRS data in 1° boxes around the aircraft. MOZAIC humidity (reported over water) is recalculated using the same merged ice and water vapor pressure formulation (Goff and Gratch 1946) as for AIRS data. For temperature and water vapor separately (not shown) results are quite good with no obvious biases throughout the range of AIRS data. However, there is significant scatter and uncertainty in both measurements. This leads to large uncertainties in individual point RH measurements. Much of this uncertainty comes from vertical gradients in humidity, particularly around the tropopause where much of the MOZAIC data is taken at flight levels but provides little information on vertical gradients (except on ascent and descent). So, for comparison purposes we again turn to a climatology, in this case for 2003, when we have a complete set of both AIRS and MOZAIC data.

Figure 5 illustrates comparisons between AIRS and MOZAIC data for 2003 for the Tropics and subtropics (30°S–30°N, Fig. 5a) and midlatitudes (40°–60°N, Fig. 5b). The AIRS supersaturation fraction is 1% in the Tropics and 6.5% in midlatitudes, while the corresponding fractions for MOZAIC are 9% in the Tropics and 18% at midlatitudes. While the fraction of points supersaturated is different, the exponential slopes are similar. The exponent of the slope for AIRS data is −0.08 (Tropics) and −0.06 (midlatitudes), and the MOZAIC slopes are −0.08 (Tropics) and −0.07 (midlatitudes). The important point is not the quantitative slope, but the exponential distribution, which is seen in

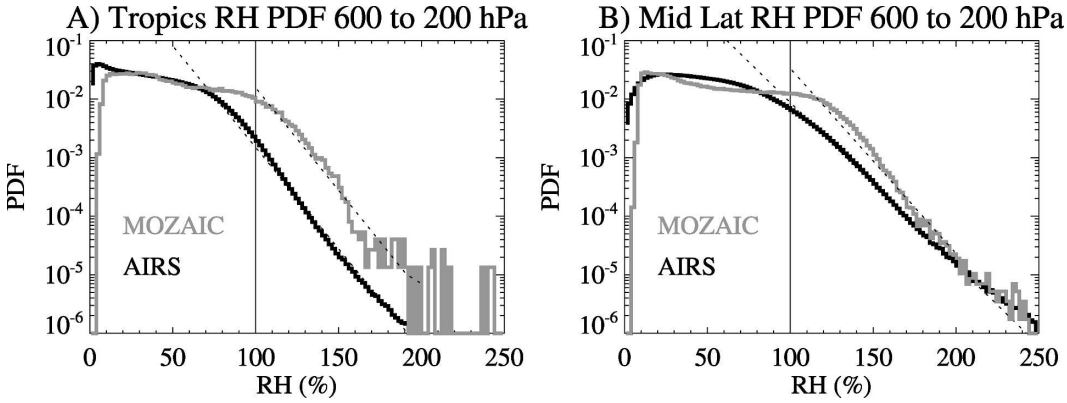

FIG. 5. PDFs of RH from AIRS for (a) the Tropics (30°S–30°N) and (b) Northern Hemisphere midlatitudes (40°–60°N). AIRS: black line, MOZAIC: gray line; dashed lines are exponential fits to the data between 100% and 200% RH.

most other data (e.g., Spichtinger et al. 2002). Gierens et al. (1999) provides a discussion of the statistical modes to explain this distribution. Buehler and Courcoux (2003) notes how uncertainties, particularly in temperature, can give rise to such a distribution.

With respect to Fig. 5, MOZAIC sees ~100% RH much more frequently than AIRS. One possible cause for this discrepancy is that MOZAIC may be seeing significant thin cirrus cloud particles, which are evaporated in the inlet before measurement, thus shifting the RH PDF toward higher values, particularly around 100% RH. Alternatively, vertical sampling issues from AIRS may be a cause of the discrepancy (e.g., when part of the AIRS averaging kernel is in the lower stratosphere). As noted, from microphysical considerations we do not expect to see RH > 160%, and values higher than this are likely due to noise in both AIRS and MOZAIC data.

We summarize these comparisons and others reported in the literature in Table 1. In addition to the MOZAIC and PreAVE observations, we also cite observations using the TOVS satellite over Europe by Gierens et al. (2004) and MLS observations at 215 hPa reported by Spichtinger et al. (2003a). In general, AIRS reports less supersaturation than most in situ sensors. It reports more supersaturation than TOVS and MLS in midlatitudes, which is not surprising given the higher vertical resolution available from AIRS. However, AIRS reports a lower frequency of supersaturation in the Tropics and globally than MLS at 215 hPa. We might expect this for two reasons: First, the low vertical resolution of MLS means that 215-hPa data includes information from higher altitudes where humidity increases rapidly around the tropical tropopause. Second, MLS is able to sound in regions of cirrus clouds, where humidity is higher and supersaturation is more likely.

In summary, despite uncertainties inherent in satellite data, upper-tropospheric supersaturation observed from AIRS appears to be consistent with in situ data. The frequencies of supersaturation are lower than observed in situ, which may be expected based on the large AIRS sampling volume. Uncertainties discussed

TABLE 1. Frequency of supersaturation.

Location	Observation source	Frequency (%)		Reference
		Observed	AIRS	
Tropics (30°S–30°N)	MOZAIC	9.3	1.1	This study
Midlatitudes (40°–60°N)	MOZAIC	18	6.5	
Tropical east Pacific	PreAVE Harvard	6.1	1.1	This study
Tropical east Pacific	PreAVE JPL LH	1.3	1.1	
Northern Europe, 300–500 hPa	TOVS	8	14	Gierens et al. (2004)
Global 90°S–90°N, 215 hPa	MLS	10.6	3.2	Spichtinger et al. (2003a)
NH: 30°–90°N	MLS	0.9	2.9	
Tropics: 30°S–30°N	MLS	18.9	2.6	
SH 90°–30°S	MLS	0.3	4.6	
Antarctic: 55°–90°S	MLS	6	3.7	

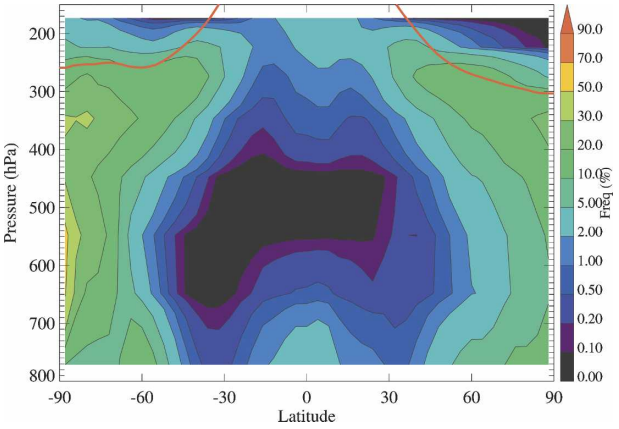

FIG. 6. Annual zonal mean frequency (%) of supersaturation by latitude and height calculated from all points. Note that the color scale is not linear. Red line is the annual zonal mean tropopause from NCEP–NCAR reanalysis data.

in section 2 would tend to increase the frequency of supersaturation. However, individually and statistically, the results compare well to available in situ data from aircraft and balloons. In general, the higher the vertical resolution, the more supersaturation is observed. This is not surprising, given a simple thought experiment. Suppose a 500-m-thick layer just below the tropopause is supersaturated, with very low humidity above it the stratosphere and subsaturated air below. Then an in situ sensor measuring within the supersaturated layer, or a remote sensor with vertical weighting of 500 m (seeing only the layer), will indicate supersaturation. A sensor with a vertical weighting of 1000 m from the tropopause down may report supersaturation, and a sensor with a vertical weighting of 1500 m (and including part of the stratosphere) is not likely to see the 500-m supersaturated layer. Thus, the frequency of supersaturation observed from AIRS has significant geophysical uncertainty. However, AIRS provides unprecedented daily global coverage with sufficient horizontal and vertical resolution to detect large-scale supersaturation, with coarse resolution reducing the amount of supersaturation observed (and "noise" increasing it).

4. AIRS climatology

In this section we use AIRS RH observations to develop a climatology of the frequency of supersaturation. We start with the annual zonal mean and then look at various regions and locations.

The annual zonal-mean frequency of supersaturation observed from AIRS is illustrated in Fig. 6. In general, the frequency of supersaturation maximizes below the extratropical tropopause (red line in Fig. 6) between 10% and 30% of the time. This value is similar to the annual mean potential contrail coverage frequency (which implies RH over ice greater than 100%) reported from ECMWF reanalyses by Sausen et al. (1998).

The frequency of supersaturation is higher in the Southern Hemisphere than the Northern Hemisphere, a point that we return to in section 5. There is rarely ever any supersaturation seen in the middle troposphere in the Tropics and subtropics (less than 0.1% of the time). There is an increase in the frequency of supersaturation at higher altitudes in the Tropics. The AIRS data does not extend high enough to resolve the tropical tropopause layer, where MLS sees high frequencies of supersaturation.

Supersaturation in the Tropics is highlighted at 200 hPa in Fig. 7. In general, higher frequencies of supersaturation are seen to follow the seasonal evolution of deep tropical convection in the upper tropical troposphere. Highest frequencies of 10%–20% are seen around the Asian monsoon in July–September (Fig. 7c), and over convective regions of Africa and South America, following the sun (and deep convection). Virtually no supersaturation is observed in the extratropical lower stratosphere or in subtropical dry regions in the upper troposphere, particularly the southeastern Pacific.

At 300 hPa (Fig. 8) the distribution of supersaturation is quite different. The subtropical subsidence regions rarely, if ever, experience supersaturation, but mid- and high latitudes in the upper troposphere, and occasionally in the lower stratosphere, experience supersaturation as much as 20%–30% of the time, while lower levels of the tropical convection regions see supersaturation less than 5% of the time. The values at midlatitudes are qualitatively similar to persistent contrail coverage (which requires supersaturation with respect to ice) as reported by Minnis et al. (2003) over regions of the continental United States with frequent aircraft traffic.

Supersaturation frequency is not zonally uniform in Fig. 8, particularly in mid- and high latitudes of the Northern Hemisphere. Less supersaturation is seen in the North Pacific in all seasons than in the North Atlantic. This is probably due to lower relative humidities (Gettelman et al. 2006), but it may also be an artifact of a lower tropopause in this region, yielding a greater influence of stratospheric air. Supersaturation is more frequent over Asia, the western region of North America, and the Atlantic in most seasons. The Southern Hemisphere has a more zonally symmetric distribution.

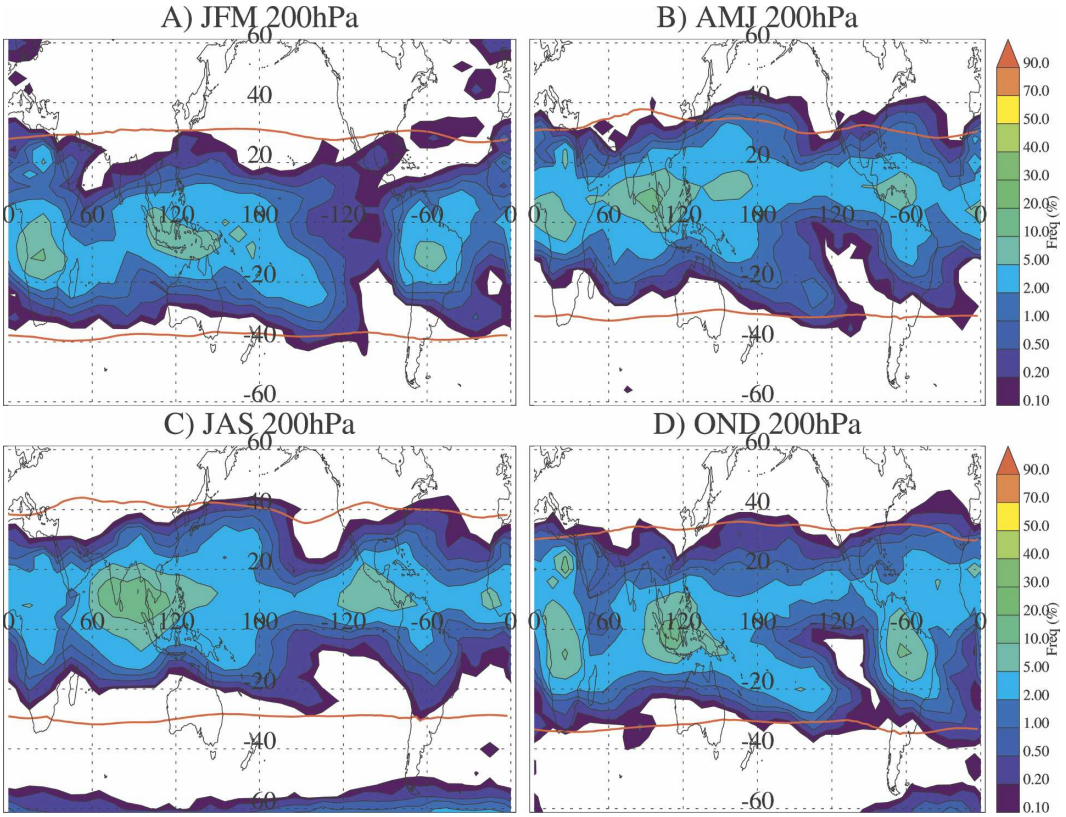

FIG. 7. Frequency of supersaturation at 200 hPa for four seasons: (a) January–March, (b) April–June, (c) July–September, and (d) October–December. Red line is the seasonal mean tropopause from NCEP–NCAR reanalysis data.

Another way to look at the data is to sort by only those points that are in the troposphere. Figure 9 illustrates the same field as Fig. 8 but sorted for only points that are at least 50 hPa below the tropopause. This removes variations due to the tropopause from the estimates. At mid- to high-latitudes supersaturation is observed at high latitudes below the tropopause nearly half the time in both hemispheres. Patterns are similar between hemispheres, but planetary wave structures are slightly different. Less supersaturation below the tropopause is seen in winter and spring in each hemisphere, and more is seen in summer (January–March in the Northern Hemisphere and October–December in the Southern Hemisphere).

Figures 8 and 9 highlight another reason why the supersaturation observed from AIRS is unlikely to be noise. Because nadir retrievals are sensitive to surface properties, AIRS temperature retrievals have higher rms errors over land (1–2 K) than over ocean (less than 1 K; Tobin et al. 2006). Thus, if temperature noise were creating spurious supersaturation, we would expect higher supersaturation frequency over land and discontinuities in coastal regions. An increase in temperature variance from 1 to 2 K would double the frequency of supersaturation. This is clearly not the case in the frequency maps in Figs. 7, 8, and 9, or for a daily map of RH in Fig. 1.

AIRS retrieves data globally, even over the poles. More data is available near the poles as the satellite orbits converge. Resolution is the same, but there are more samples per day. Figure 10 illustrates the frequency of supersaturation near the surface over both poles (600 hPa in the Southern Hemisphere over the Antarctic ice cap, 850 hPa over the north polar region). Over the Antarctic ice cap (Fig. 10a), supersaturation is observed over 70% of the time, while over the North Polar region, supersaturation is observed 10%–20% of the time. Extremely cold temperatures over Antarctica may be a reason for this difference. It is likely that over Antarctica in winter the regime is always one of pure ice saturation near the surface (temperatures below −40°C) whereas over the North Polar region mixed phase processes at higher temperatures may be acting.

While the AIRS record only spans 31 months, data over 2.5 annual cycles allows some analysis of the repeatability of the annual cycle. Figure 11 illustrates the

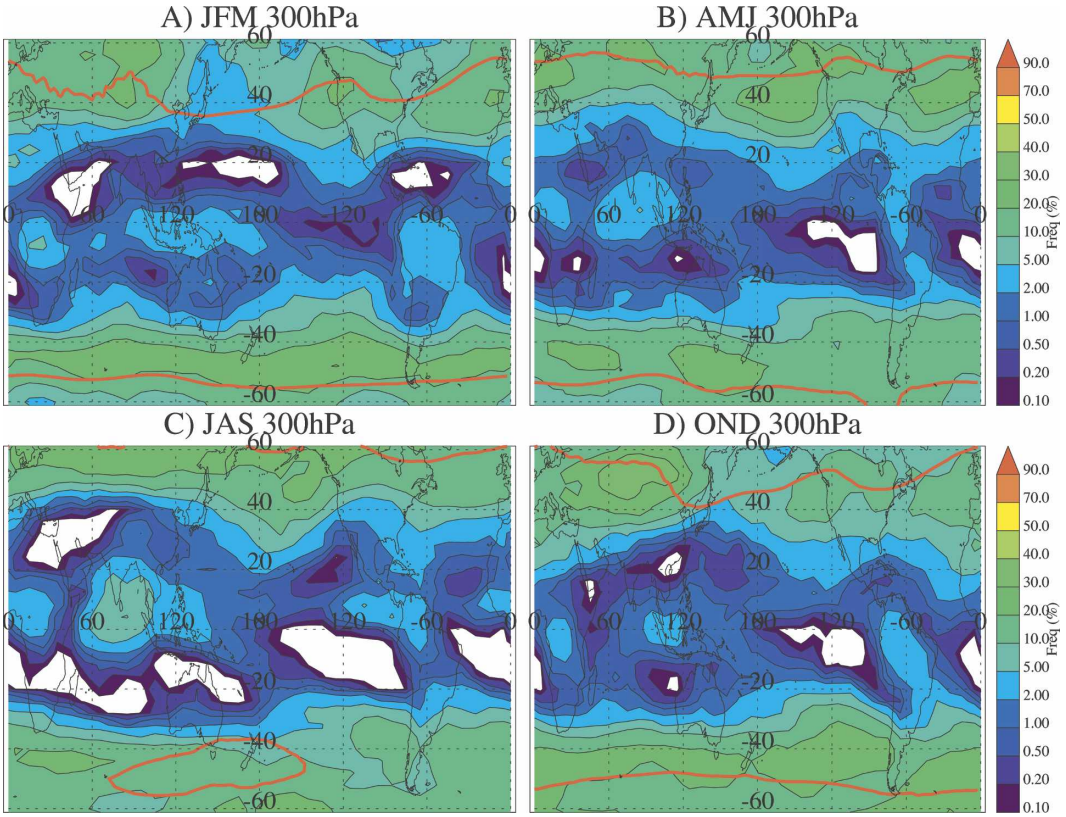

FIG. 8. As in Fig. 7 but at 300 hPa.

supersaturation fraction in percent for four regions. These estimates are made using only points in the troposphere, similar to Fig. 9. In general, there is a reproducible annual cycle at all four locations. The most variation year to year is seen in the Southern Hemisphere midlatitude upper troposphere (Fig. 11b), which also has the highest frequency of supersaturation.

As indicated in Fig. 6 and Fig. 11, there is more supersaturation in the midlatitude upper troposphere in the Southern Hemisphere (Fig. 11b) than in the Northern Hemisphere (Fig. 11c). Figure 12 illustrates the PDFs for each hemisphere, highlighting the difference. Ovarlez et al. (2002) observed higher relative humidities in the Southern Hemisphere than the Northern Hemisphere during fall on a limited basis with in situ measurements during the INCA campaign and attribute the difference to higher levels of pollution in the Northern Hemisphere, which imply more ice nuclei and more heterogeneous nucleation of clouds at lower RHi than for homogeneous nucleation.

Data in Ovarlez et al. (2002) indicate that outside of clouds (where AIRS sees) relative humidities greater than 105% were observed 23% of the time in the Southern Hemisphere and 9% of the time in the Northern Hemisphere during fall for one region in each hemisphere. AIRS data in Fig. 12 for a hemispheric average of the latitude band 40°–60° indicate supersaturation 8% of the time in the Southern Hemisphere and 6% in the Northern Hemisphere. If only points in the troposphere are considered, the values are 17% and 12% for the Southern and Northern Hemispheres, respectively. These values are comparable to the INCA out of cloud data, especially considering that we expect lower frequencies due to the vertical resolution of AIRS. The hemispheric differences are less in this study than in Ovarlez et al. (2002), probably owing to the larger sampling volume in space and time of the AIRS data.

5. Discussion

AIRS RH shows significant regions of supersaturation, to the extent that it is visible from a satellite. Statistically, it is possible that much of the observed supersaturation could be due to random errors in temperature and specific humidity observations, if they are normally distributed and uncorrelated. Statistical uncertainties tend to increase the supersaturation observed by AIRS, while the large sampling volume tends to reduce the observed frequency of supersaturation. We have several reasons for concluding that at least

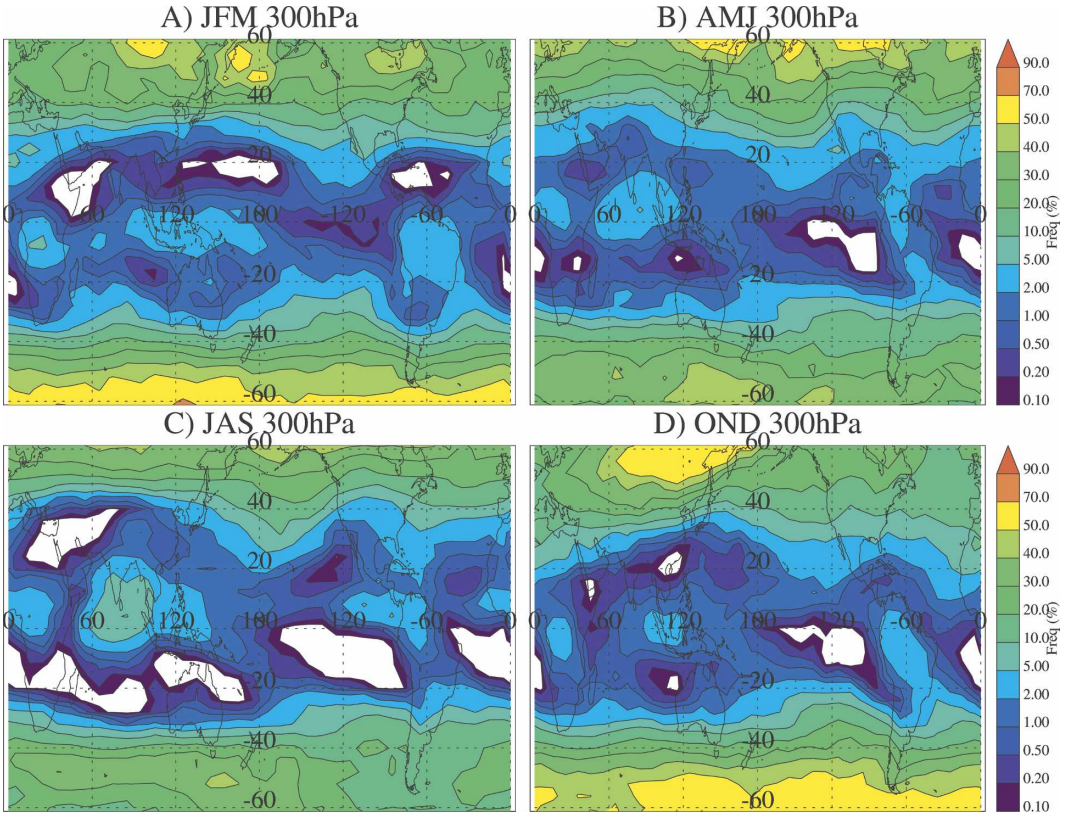

FIG. 9. As in Fig. 8 but in the upper troposphere for data points below the tropopause.

some supersaturation is seen from AIRS. First, regions of observed supersaturation from AIRS are coherent on daily to seasonal time scales and occur in geophysically realistic locations. Second, AIRS data are consistent with other analyses and agree quite well with statistical distributions from in situ aircraft and balloons in similar regions, or with regions of persistent contrails. Frequencies of supersaturation are less than in situ observations, likely due to the large sample volume represented by AIRS (45 km × 45 km × 2 km), which may miss the significant fraction of events on a smaller scale. Finally, the frequency of supersaturation observed from AIRS does not resemble the known land–sea contrast of the retrieval uncertainty. If noise in either the temperature or water vapor retrieval were causing most of the supersaturation in AIRS data, we would expect

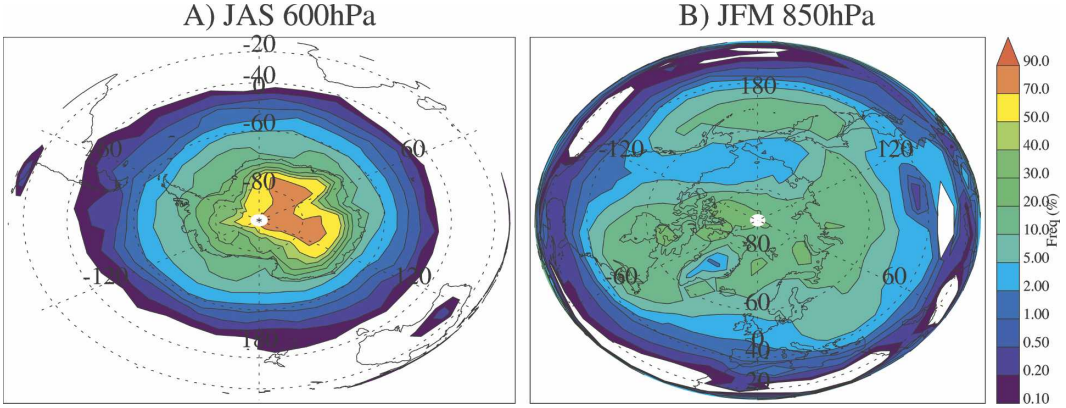

FIG. 10. Frequency of supersaturation in the lower troposphere for (a) the South Pole at 600 hPa in July–September and (b) the North Pole at 850 hPa in January–March.

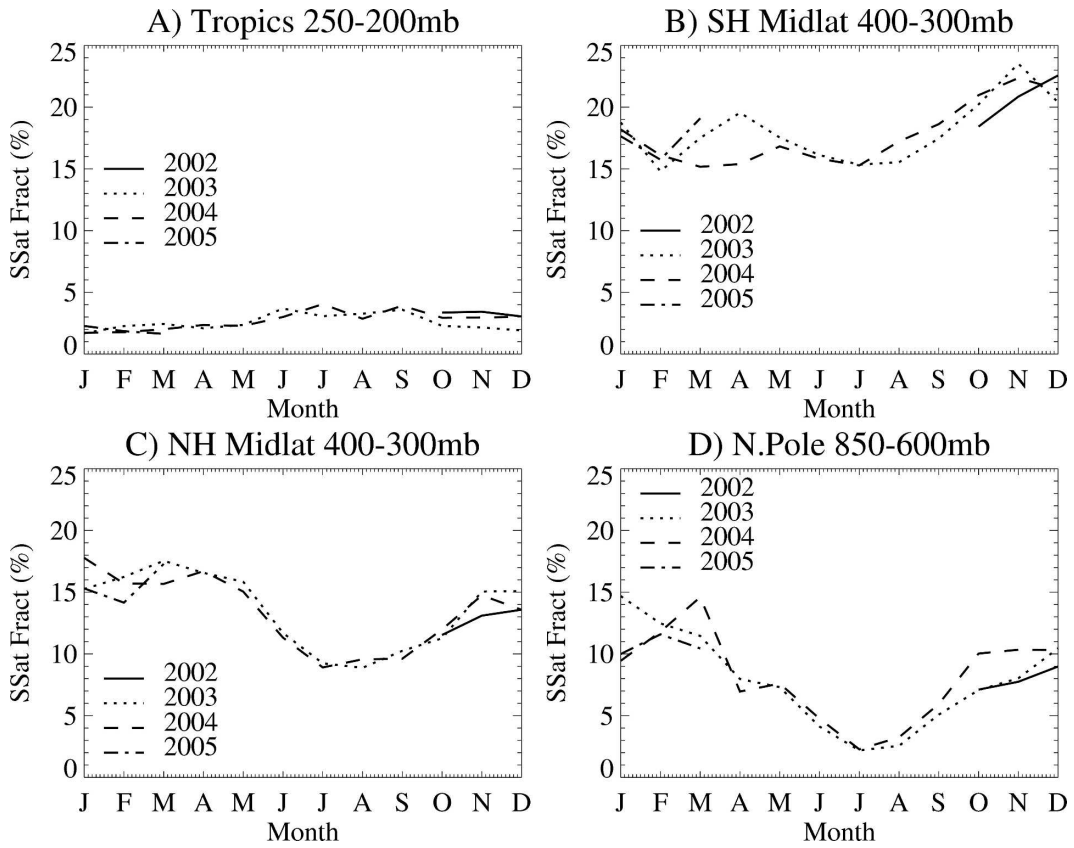

FIG. 11. Frequency of supersaturation in the upper troposphere for each month of the year in four different regions observed by AIRS: (a) the Tropics (10°S–10°N) at 250–200 hPa, (b) Southern Hemisphere (60°–40°S) at 400–300 hPa, (c) Northern Hemisphere (40°–60°N) at 400–300 hPa, and (d) North Pole (70°–90°N) at 850–600 hPa. Different years shown: 2002 (solid), 2003 (dotted), 2004 (dash), and 2005 (dot–dash).

much higher supersaturation frequency over land (up to twice as much), which is not observed.

As a result of this large sampling volume and uncertainty, it is difficult to relate supersaturation observed from AIRS quantitatively with details of cloud microphysics (i.e., the critical supersaturation for ice nucleation). The "relative humidity" observed by AIRS is really a "bulk" relative humidity, and no doubt varies significantly within the sampling volume. This is particularly true in the vertical, as the upper troposphere is a region of strong vertical gradients in water vapor, either due to the tropopause or vertical shear in the horizontal wind, which creates significant stirring and layering. Thus it is not appropriate to quantitatively discuss the implications of supersaturation observed from satellites for cloud formation. However, we can discuss the implications of the climatology of bulk supersaturation, which is relevant for understanding the persistence of contrails and cirrus clouds.

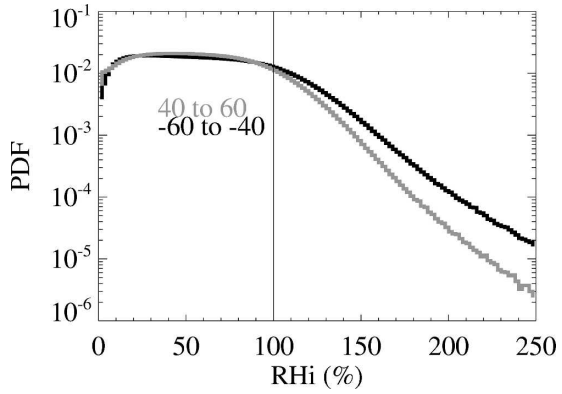

FIG. 12. PDFs of RH from AIRS in the upper troposphere (400–200 hPa) in the midlatitudes of the Southern (black) and Northern (gray) Hemispheres.

Overall, AIRS data paint a coherent picture of supersaturation in the upper troposphere. Relative humidity and the frequency of supersaturation increase with altitude in the upper tropical troposphere but, since AIRS is unable to resolve values above 200 hPa, it is not clear how much supersaturation is present in

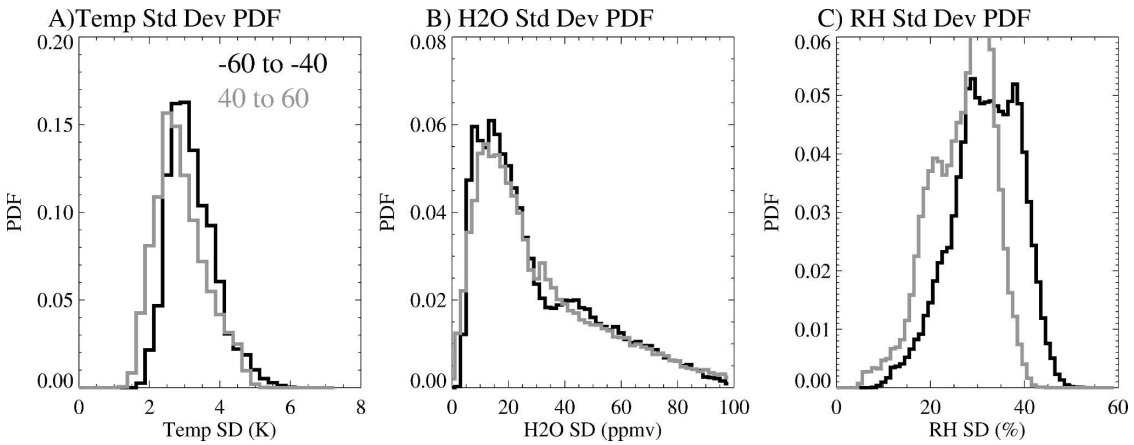

FIG. 13. PDFs of the standard deviation of (a) temperature, (b) water vapor, and (c) relativew humidity from 31 months of AIRS data in the upper troposphere (300–250 hPa) in the midlatitudes (40°–60° latitude) of the Southern (black) and Northern (gray) Hemispheres.

the Tropical tropopause layer. In the subtropics, very little supersaturation is seen. Seasonally, supersaturation in the upper tropical troposphere follows major regions of convection (and the supply of humidity).

In middle and high latitudes, there is significant supersaturation near the tropopause, especially in the regions of storm tracks. Highest frequencies in the upper troposphere (Fig. 9) are found in spring and summer. In polar regions (Fig. 10), supersaturation is often seen near the surface as well, particularly in winter, and is quite high over the Antarctic ice cap.

AIRS data also show hemispheric differences in supersaturation, with more supersaturation in the Southern Hemisphere (Fig. 12). Ovarlez et al. (2002) make the claim that this difference is likely due to enhanced pollution in the Northern Hemisphere observations, which were taken in the North Atlantic off the coast of Ireland, whereas the observations from the Southern Hemisphere were taken off the coast of South America. AIRS data indicate that the differences are general and hemispheric. However, it is not clear that this is due to enhanced ice nuclei from anthropogenic sources. An examination of Fig. 8 indicates for example that the northeastern Pacific and the North Atlantic have similar frequencies of supersaturation (10%–40% depending on season). As the northeastern Pacific is likely cleaner, it should have more supersaturation if anthropogenic pollution dominates the frequency of supersaturation.

It appears more likely from AIRS data that there is simply a larger variance in temperature in the Southern Hemisphere, which leads to a larger variance in relative humidity. As Fig. 3 makes clear when applied to a simulated distribution, adding variability to RH tends to broaden the RH distribution. There is also good correspondence between the regions of supersaturation in Fig. 8 and regions of high RH variance (see Gettelman et al. 2006, Fig. 5). Because RH is linear with respect to water vapor but exponential with respect to temperature (due to the dependence of saturation vapor pressure in the Clausius–Clapeyron equation), relative humidity variance is more sensitive to temperature variance. This point is discussed using theoretical distributions by Kärcher and Haag (2004).

Figure 13a illustrates that AIRS temperature data show more variance in the Southern Hemisphere. A theoretical analysis of perturbations using these distributions indicate that increasing the standard deviation of temperature by 1 K can double the frequency of supersaturation, consistent with Buehler and Courcoux (2003). There is little difference in the standard deviation of water vapor observed from AIRS (Fig. 13b) and quite a large difference in RH variance (Fig. 13c) between the hemispheres. It is not clear why there should be larger temperature variance at a given level in the Southern Hemisphere. Furthermore, there is not a clear correlation between regions of higher temperature variance and higher supersaturation. Nonetheless, the data in Fig. 13 is suggestive of a link that does not require aerosols, and does not seem to be correlated with geographical variations in aerosol sources. We hesitate to speculate further because satellite observations of supersaturation are themselves sensitive to the temperature variance or uncertainty, as discussed in section 2 and by Buehler and Courcoux (2003). More detailed studies including humidity as well as aerosol observations will be necessary to fully understand these differences in supersaturation.

6. Conclusions

AIRS RH observations are a unique dataset to study supersaturation in the upper troposphere. AIRS RH data have similar distributions to in situ aircraft data from research aircraft (PreAVE) and commercial aircraft (MOZAIC), or balloons. The overall frequency of supersaturation from AIRS up to the limit of its range (200 hPa) is qualitatively consistent with other observations from satellites (Spichtinger et al. 2003b) and from estimates of potential contrail coverage from observations (Minnis et al. 2003) and reanalysis (Sausen et al. 1998).

AIRS RH is not a pointwise measurement and observed supersaturation may not quantitatively define what an air parcel or a cloud/ice nucleus experiences. Statistical uncertainties mean that we must treat the data with extreme caution, but it is plausible from the size of supersaturated regions that AIRS can observe supersaturation, and it appears likely from comparisons to in situ data that some of the supersaturation is real. The results do not have the characteristics of retrieval noise. Our conclusions are not dependent upon the specific quantitative frequency of supersaturation observed from AIRS.

In AIRS data, supersaturation appears to be very common in the upper troposphere just below the tropopause in midlatitudes, often at the leading edge of frontal systems. While AIRS does not observe the tropical tropopause layer, it appears from other data that supersaturation is also common near the tropical tropopause. There is extensive supersaturation near the surface in polar regions. There are distinct patterns to saturated air, with higher frequencies in storm track regions in midlatitudes. The annual cycle in the frequency of supersaturation is repeatable from the several years of AIRS data.

These data strongly suggest that much of the upper troposphere frequently experiences supersaturation over ice. Most global models of the atmosphere do not represent this process. Models need to properly represent the ice nucleation process if we are to understand the global impact of ice clouds and possible perturbations to ice nucleation processes by anthropogenic ice nuclei. AIRS observations may help constrain global parameterizations of cloud formation processes.

AIRS observations indicate higher frequency of supersaturation in the Southern Hemisphere midlatitude upper troposphere, consistent with limited aircraft observations. However, geographic variations of the frequency of supersaturation show little correspondence with zonal patters of anthropogenic ice nuclei, theorized to affect the hemispheres differently. Rather, the higher frequency of supersaturation is consistent with hemispheric and regional differences in temperature variance, which would lead to a broader distribution of RH and more supersaturation. AIRS temperature data are consistent with this hypothesis on a hemispheric basis, but correlations are not precise. Further, more detailed studies to supplement the global picture are desirable.

Further studies of supersaturated conditions from AIRS may be able to shed some light on cloud nucleation processes when combined with other satellite sensors. If done properly, an integrated retrieval algorithm will directly produce relative humidity (as well as specific humidity and temperature) with uncertainties lower than this method. Using an updated AIRS retrieval and cloud properties from a suite of sensors flying in formation on NASA's A-Train [such as the Moderate Resolution Imaging Spectroradiometer (MODIS) and CloudSat], we may be able to examine these important questions of ice nucleation and its global impact, as well as improve global models to examine perturbations to the earth system.

Acknowledgments. The authors would like to acknowledge the assistance of the whole AIRS team, including E. Fishbein at the NASA/Caltech Jet Propulsion Laboratory. Summaries of balloon data were provided by H. Vömel. MOZAIC aircraft data was made available by J.-P. Cammas and H. Smit. Aircraft humidity data was supplied by R. L. Herman (JPL LH) and E. M. Weinstock (Harvard). K. H. Rosenlof assisted with aircraft temperature data. Thanks to M. Park, W. Randel, and S. Massie for comments, and K. Gierens, P. Spichtinger, and S. Buehler for discussions. This research was supported under NASA Grant EOS-03-0594-0572.

REFERENCES

Appleman, H. S., 1953: The formation of exhaust condensation trails by jet aircraft. *Bull. Amer. Meteor. Soc.,* **34,** 14–20.

Aumann, H. H., and Coauthors, 2003: AIRS/AMSU/HSB on the Aqua mission: Design, science objectives, data products, and processing systems. *IEEE Trans. Geosci. Remote Sens.,* **41,** 253–264.

Brewer, A. W., 1946: Condensation trails. *Weather,* **1,** 34–40.

Buehler, S., and N. Courcoux, 2003: The impact of temperature errors on perceived humidity supersaturation. *Geophys. Res. Lett.,* **30,** 1759, doi:10.1029/2003GL017691.

Collins, W. D., and Coauthors, 2006: The formulation and atmospheric simulation of the Community Atmosphere Model Version 3 (CAM3). *J. Climate,* **19,** 2144–2161.

Divakarla, M. G., C. D. Barnet, M. D. Goldberg, L. M. McMillin, E. Maddy, W. Wolf, L. Zhou, and X. Liu, 2006: Validation of Atmospheric Infrared Sounder temperature and water vapor

retrievals with matched radiosonde measurements and forecasts. *J. Geophys. Res.,* **111,** D09515, doi:10.1029/2005JD006116.

Fetzer, E., and Coauthors, 2003: AIRS/AMSU/HSB validation. *IEEE Trans. Geosci. Remote Sens.,* **41,** 418–431.

Gettelman, A., and Coauthors, 2004: Validation of Aqua satellite data in the upper troposphere and lower stratosphere with in situ aircraft instruments. *Geophys. Res. Lett.,* **109,** L22107, doi:10.1029/2004GL020730.

——, W. D. Collins, E. J. Fetzer, A. Eldering, F. W. Irion, P. B. Duffy, and G. Bala, 2006: Climatology of upper-tropospheric relative humidity from the Atmospheric Infrared Sounder and implications for climate. *J. Climate,* **19,** 6104–6121.

Gierens, K., and P. Spichtinger, 2000: On the size distribution of ice supersaturation regions in the upper troposphere and lower stratosphere. *Ann. Geophys.,* **18,** 499–504.

——, U. Schumann, M. Helten, H. Smit, and A. Marenco, 1999: A distribution law for relative humidity in the upper troposphere and lower stratosphere derived from three years of MOZAIC measurements in the upper troposphere and lower stratosphere. *Ann. Geophys.,* **17,** 1218–1226.

——, ——, ——, ——, and P.-H. Wang, 2000: Ice-supersaturated regions and subvisible cirrus in the northern midlatitude upper troposphere. *J. Geophys. Res.,* **105,** 22 743–22 754.

——, R. Kohlhepp, P. Spichtinger, and M. Schroedter-Homscheidt, 2004: Ice supersaturation as seen from TOVS. *Atmos. Chem. Phys.,* **4,** 539–547.

Glückauf, E., 1945: Notes on upper air hygrometry-II: On the humidity in the stratosphere. *Quart. J. Roy. Meteor. Soc.,* **71,** 110–112.

Goff, J. A., and S. Gratch, 1946: Low-pressure properties of water from −160°F to 212°F. *Trans. Amer. Soc. Heat. Vent. Eng.,* **52,** 95–121.

Helten, M., H. G. J. Smit, W. Sträter, D. Kley, P. Nedelec, M. Zöger, and R. Busen, 1998: Calibration and performance of automatic compact instrumentation for the measurement of relative humidity from passenger aircraft. *J. Geophys. Res.,* **103,** 25 643–25 652.

Heymsfield, A. J., L. M. Miloshevich, C. Twohy, G. Sachse, and S. Oltmans, 1998: Upper-tropospheric relative humidity observations and implications for cirrus ice nucleation. *Geophys. Res. Lett.,* **25,** 1343–1346.

Jensen, E. J., W. G. Read, J. Mergenthaler, B. J. Sandor, L. Pfister, and A. Tabazadeh, 1999: High humidities and subvisible cirrus near the tropical tropopause. *Geophys. Res. Lett.,* **26,** 2347–2350.

——, and Coauthors, 2000: Prevalence of ice supersaturated regions in the upper troposphere: Implications for optically thin ice cloud formation. *J. Geophys. Res.,* **106,** 17 253–17 266.

——, and Coauthors, 2005: Ice supersaturations exceeding 100% at the cold tropical tropopause: Implications for cirrus formation and dehydration. *Atmos. Chem. Phys.,* **5,** 851–862.

Kärcher, B., and W. Haag, 2004: Factors controlling upper tropospheric relative humidity. *Ann. Geophys.,* **22,** 705–715.

Kelly, K. K., M. H. Proffitt, K. R. Chan, M. Loewenstein, J. R. Podolske, S. E. Strahan, J. C. Wilson, and D. Kley, 1993: Water vapor and cloud water measurements over Darwin during the STEP 1987 tropical mission. *J. Geophys. Res.,* **98,** 8713–8723.

Marenco, A., and Coauthors, 1998: Measurement of ozone and water vapor by Airbus in-service aircraft: The MOZAIC airborne program, an overview. *J. Geophys. Res.,* **103,** 25 631–25 642.

May, R. D., 1998: Open-path, near-infrared tunable diode laser spectrometer for atmospheric measurements of H_2O. *J. Geophys. Res.,* **103,** 19 161–19 172.

Miloshevich, L. M., H. Vömel, D. N. Whiteman, B. M. Lesht, F. J. Schmidlin, and F. Russo, 2006: Absolute accuracy of water vapor measurements from six operational radiosonde types launched during AWEX-G, and implications for AIRS validation. *J. Geophys. Res.,* **111,** D09510, doi:10.1029/2005JD006083.

Minnis, P., J. K. Ayers, M. L. Nordeen, and S. P. Weaver, 2003: Contrail frequency over the United States from surface observations. *J. Climate,* **16,** 3447–3462.

Murphy, D. M., and T. Koop, 2005: Review of the vapour pressure of ice and supercooled water for atmospheric applications. *Quart. J. Roy. Meteor. Soc.,* **131,** 1539–1565.

Ovarlez, J., J. F. Gayet, K. Gierens, J. Strom, H. Ovarlez, F. Auriol, R. Busen, and U. Schumann, 2002: Water vapor measurements inside cirrus clouds in Northern and Southern hemispheres during INCA. *Geophys. Res. Lett.,* **29,** 1813, doi:10.1029/2001GL014440.

Read, W. G., and Coauthors, 2001: UARS microwave limb sounder upper tropospheric humidity measurement: Method and validation. *J. Geophys. Res.,* **106,** 32 207–32 258.

Sausen, R., K. Gierens, M. Ponater, and U. Schumann, 1998: A diagnostic study of the present and future coverage by contrails part I: Present day climate. *Theor. Appl. Climatol.,* **61,** 127–141.

Schumann, U., 1996: On conditions for contrail formation from aircraft exhausts (review article). *Meteor. Z.,* **5,** 4–23.

Spichtinger, P., K. Gierens, and W. Read, 2002: The statistical distribution law of relative humidity in the global tropopause region. *Meteor. Z.,* **11,** 83–88.

——, ——, U. Leiterer, and H. Dier, 2003a: Ice supersaturation in the tropopause region over Lindenberg, Germany. *Meteor. Z.,* **12,** 143–156.

——, ——, and W. Read, 2003b: The global distribution of ice-supersaturated regions as seen by the Microwave Limb Sounder. *Quart. J. Roy. Meteor. Soc.,* **129,** 3391–3410.

Susskind, J., C. D. Barnet, and J. M. Blaisdell, 2003: Retrieval of atmospheric and surface parameters from AIRS/AMSU/HSB data in the presence of clouds. *IEEE Trans. Remote Sens.,* **41,** 390–409.

Tobin, D. C., and Coauthors, 2006: Atmospheric Radiation Measurement site atmospheric state best estimates for Atmospheric Infrared Sounder temperature and water vapor retrieval validation. *J. Geophys. Res.,* **111,** D09514, doi:10.1029/2005JD006103.

Vömel, H., and Coauthors, 2002: Balloon-borne observations of water vapor and ozone in the tropical upper troposphere and lower stratosphere. *J. Geophys. Res.,* **107,** 4210, doi:10.1029/2001JD000707.

Weinstock, E. M., and Coauthors, 1994: New fast response photofragment fluorescence hygrometer for use on the NASA ER-2 and the Perseus remotely piloted aircraft. *Rev. Sci. Instrum.,* **65,** 3544–3554.